GASEOUS OXYGEN AND HYDROGEN EMBRITTLEMENTS OF A U-10 Mo ALLOY

J. Corcos, A. M. Nominé and D. Miannay*

INTRODUCTION

Uranium alloys with high molybdenum or niobium content can retain their high temperature stable body-centered-cubic structure γ at low temperature by quenching. Their mechanical resistance is high and they have much more oxydation and corrosion resistance than leaner alloys. However they are very susceptible to stress corrosion cracking (S.C.C.). For uranium-molybdenum binary alloys, the phenomenology of this cracking is largely documented in the literature [1 - 7]: at temperature near the ambient this phenomenon occurs under external loading or residual stresses in air with varying humidity [1], [3 - 7], in water with or without the presence of Cl^- [5, 6], in oxygen and hydrogen gaseous environments at atmospheric pressure [1, 3, 4]; nitrogen and helium gases are said to be innocuous [3]; in the range 300 to 400°C, Burkhart and Lustman [2] describe a type of S.C.C. based on the formation and fracture of brittle, uranium base hydrides in U-12 Mo alloy which is stressed and exposed to steam and water.

For the first type of cracking, in air, oxygen or hydrogen released from the reaction of water vapor with the alloy are the species responsible. The phenomenon is thermally activated in U-5 Mo with a 6.3 $kcal.mole^{-1}$ activation energy [1]. The effect upon ductility is more pronounced at low strain rates and is suppressed above a threshold rate varying with alloying content. The embrittlement is thought to be diffusion controlled with dislocations dragging interstitial hydrogen and the diffusivity of hydrogen in U-10 Mo at room temperature will be $5.10^{-11} cm^2.s^{-1}$ [7], lower than the lattice diffusivity of hydrogen in a similar alloy U-7.5Nb.2_p5Zr, i.e., $3.10^{-8} cm^2.s^{-1}$ [8]. However, addition of titanium, zirconium or niobium which can trip hydrogen are found to be without effect [6, 9, 10]. Addition of humidity will be deleterious [4]. In oxygen gas, there is a threshold pressure below which no cracking occurs in U-5 Mo. For U-10 Mo, additions of moisture will be deleterious according to Sulsona [4] and beneficial according to Peterson [3]. In hydrogen gas, the susceptibility to cracking of U-10 Mo is enhanced by humidity. The stress-strain behaviour of U-10 Mo is unaffected in vacuum, air and oxygen [3].

The purpose of this paper is to contribute to the understanding of the mechanisms of gaseous hydrogen and oxygen embrittlements of U-10 Mo by studying the kinetics of crack growth using fracture mechanics to describe the state of stresses at the tip of a crack.

* Commissariat à l'Energie Atomique, Centre d'Etudes de Bruyères-le-Châtel, B.P. No. 511-15-75015 Paris, France

ALLOY AND EXPERIMENTAL PROCEDURE

The bulk chemical analysis of the cast U-10 Mo alloy used in these experiments is shown in Table 1. Coupons of dimensions 80 mm x 20 mm x 5 mm were given the standard heat treatment: a γ solution anneal at 1000°C during 24 hours under vacuum, followed by a quench to room temperature, furnace removed and air flowing on the laboratory tube. The resulting structure has a typical grain size of 450 µm and is single phase.

Crack growth data were obtained using 72 mm x 18 mm x 4 mm single edge cracked specimens which were machined from the heat treated coupons. Fatigue precracking was done in dehumidified nitrogen in a closed test chamber at stress intensity levels of about K_f = 11 MPa•m$^{1/2}$ with ΔK_f = 7 MPa•m$^{1/2}$. The sustained load testing was carried out in tension in the same chamber and the crack growth was monitored by observation of a specimen face through a window using optical microscopy.

The test environment was dehumidified high purity hydrogen or oxygen gases flowing at 0.15 MPa pressure at a rate of 10 ℓ.hr^{-1}. Before testing, residual impurities were minimized by heating the chamber and supply system to 20°C above the testing temperature and purging with dehumidified high purity nitrogen. The gas was introduced at room temperature. The hydrogen was purified by passage through a heated palladium-silver thimble and the oxygen through a molecular sieve. The impurity level measured with a hygrometer and a chromatograph is below 1 vpm. Some experiments were done at 20°C with oxygen partial pressures of 1.5 kPa, obtained by using oxygen-nitrogen gas mixtures. The influence of temperature was examined over the range from 0°C to + 100°C for oxygen and from + 20°C to + 132°C for hydrogen. The loading is done in about 2 mn when the temperature is obtained after about 1 hr and this temperature is monitored with a stability of ± 2°C by a thermocouple located in the notch.

When no crack growth was visible after 2000 hours, the test was stopped and was said to have been conducted below K_{ISCC}. Load was then removed, flowing dehumidified nitrogen was sent on the specimen until all the testing gas is removed and reloading is done up to brittle fracture with a rate of about 0.2 MPa•m$^{1/2}$s^{-1}. The fracture surface was then studied using scanning electron fractography to determine if there was any stress corrosion crack propagation.

In these tests, plane strain conditions were achieved when dimensions were larger than $(K_I/\sigma_y)^2$ [11]. This limit is drawn on the next figures for typical values of K_{IC}.

Additional experiments were aimed at locating and identifying the embrittling species using optical metallography, electron and ion microprobe analysis, and X-Ray analysis of cross-sections of the fractures. Fractography was also used.

GASEOUS OXYGEN EMBRITTLEMENT

Figure 1a shows the range of initial stress intensity factors and of temperatures where failure takes place in 2000 hr: K_{ISCC} is close to K_{IC} at 0°C, it decreases with increasing temperature up to 60°C and above, it increases with temperature. However, when no cracking is observed on the fracture surface in the 0°C and the 60°C, 10 MPa•m$^{1/2}$ tests, some internal S.C.C. is observed in the 40°C, 80°C and 100°C tests with

K_{Ii} = 20 MPa•m$^{1/2}$, the extent of which is decreasing with increasing temperature. This observation with the fact that there is an incubation time decreasing with increasing temperature and initial stress intensity K_{Ii} may throw some doubt about the true significance of the apparent value of K_{ISCC}. Moreover, it suggests that cracking initiates in the centre of the testpiece's piece thickness B where plane strain conditions prevail and advances by both tunneling into the centre and spreading in the through thickness direction. And in the 60°C, 30 MPa•m$^{1/2}$ test some growth with high plasticity has been observed before stopping after 18 hours: no explanation can be yet given.

Propagation as observed on the surface is discontinuous with roughly three stages: after a relatively fast transient period with building of a plastic zone, cracking slows down and then accelerates more and more when approaching failure. The variation of growth rate da/dt versus K_I as obtained after neglecting the transient period and fitting a smooth curve to data points is shown in Figure 1a: the rate appears to be nearly insensitive to K_I; a thermally activated mechanism seems to be indicated and the linear Arrhenius relation gives an apparent activation energy of about 8 kcal/mole. Rate appears to be lightly enhanced at low pressure. K_{IS} at instability after cracking, measured from crack surface observation, as shown in Figure 1, is much more than K_{Ic} and even in the 20°C, 25 MPa•m$^{1/2}$, 1.5 10^{-2} atm. test, S.C.C. has occurred all through the specimen: this phenomenon is very often encountered in S.C.C. [12].

After loading, the plastic zone builds up around the tip and its size measured on either side of the crack agrees closely with the value calculated from elastic-plastic analysis, $r_{p,max} = 0.15(K_I/\sigma y)^2$ in plane strain [13]. Then (Figure 2a), plasticity spreads from the ends of the plastic fans for a further distance at each end. According to the specimen, one of these plastic bands coarsens when going close to the normal propagation direction or these bands join in advance of the crack tip on this direction and then coarsen. After this stage, propagation occurs along these bands and goes on with and without plasticity, suggesting that either the yield stress of the material ahead of the crack tip is increased during subcritical cracking or the local stress intensity does not increase continuously with increasing applied stress intensity or the strain distribution is not the same for a continuously advancing crack than for a stationary one. The crack path is transgranular with a crystallographic type which is identified by X-Ray analysis as (111), the same as in air [6]. When K_I goes over K_{Ic}, extensive plasticity takes place with some grain boundary cracking in it.

Observation of fracture surface shows the flat, quasi-cleavage fracture mode with some dimples probably occurring by ductile tearing due to overload between adjacent cleavage planes below about K_{Ic}, which is characteristic of air cracking in U-Mo alloys, and with intergranular fracture without evidence of corrosion attack above this threshold. No branching nor crevices are observed except under low pressure, low K_{Ii} and high K_I. After this region, the normal type of unstable fracture with the dimple mode the extent of which varies with temperature and with the intergranular mode is observed.

To account for the onset of propagation we propose the following model (Figure 2b): crack propagates at first in the interior where crack closure is less [14] and when it approaches the external surface, plastic relaxation takes place on lines transverse to the sheet surface at 45° to the tensile axis. Due to the absence of strain-hardening of the alloy

and the interaction of internal slip step emergence with oxygen, which may be assumed responsible for cracking, one system is developing during growth until rupture if no overload occurs as in unstable fracture. When plastic zone size becomes very large, the normal rupture mode appears and may be promoted or prevented by oxygen. Since the oxide thickness is about 10 A, the brittle film-rupture mechanism is dismissed, oxygen is thought either to decrease the surface energy or to increase locally the yield stress.

GASEOUS HYDROGEN EMBRITTLEMENT

The S.C.C. map and the enhanced crack growth rate are shown in Figure 1b: all specimens failed even under no load; the rate can vary slowly below $K_I \simeq 20$ MPa•m$^{1/2}$ and is fairly constant above this level; this rate is thermally activated under no load between 20°C and 132°C and under load between 60°C and 100°C with an apparent activation energy of 8 kcal/mole. These results must be considered as preliminary because hydrogen enhanced crack growth in maraging steels is reported with a critical temperature for describing two kinds of behaviour of the rate with temperature [15]. The incubation time follows no definite trend with temperature nor K_I and is often 0. Moreover, for the 60°C, 20 MPa•m$^{1/2}$ test, the rate is lower than for the 60°C, 15 MPa•m$^{1/2}$ test, a phenomenon previously reported for the U - 0.75 w% Ti cracking in H_2 [16].

At low K_{Ii} or K_I (Figure 3), reaction occurs in the residual and applied tensile regions of the crack tip. This reaction is followed by extensive plasticity which drags hydrogen to near grain boundaries where new transgranular reaction or precipitation occurs along with some coherency. Due to assumed wedging action of this second precipitate, fracture occurs at each end and very active gettering takes place at the fresh crack surface. Then, the processus is repeated. At high K_{Ii}, the plastic zones form at the tip and cracking occurs within them where high shear strains must be sustained under a tensile stress. Macroscopic branching follows. At high K_I, under growing plasticity, general intergranular decohesion takes place and precipitation follows.

On cross-sections three kinds of precipitates with uranium and hydrogen are revealed: intergranular and transgranular coarse precipitates with molybdenum, a Widmanstätten structure without molybdenum and small precipitates at grain boundaries and along wavy slip lines. Spalled powder was identified as a body centered cubic phase with $a_o = 4.18.10^{-10}$m, very close to $UH_3\alpha$.

Embrittlement is thought to be due to brittle hydride formation and hydrogen pressure buildup at grain boundaries. The phenomenon is complicated by varying pressure at the extending crack tip, lower than the bulk pressure due to limited hydrogen transport and by enhanced hydrogen solubility and diffusivity due to plasticity and grain boundaries.

REFERENCES

1. PRIDGEON, J. W., Report Y.1417, O.R.N.L., May, 1963.
2. BURKHART, M. W. and LUSTMAN, B., Trans. AIME, 26, 1958.
3. PETERSON, C. A. W. and VANDERVOORT, R. R., U.C.R.L. 7767, March, 1964.
4. SULSONA, H., Ph. D. Thesis, University of Arizona, 68, 12, 1968, 922.
5. MAGNANI, N. J., Corrosion 72, NACE, Paper No. 58, 1972.

6. NOMINÉ, A. M., BÉDÈRE, D. and MIANNAY, D., Facteurs mécaniques et métallurgiques de la rupture, CEN Saclay, France, 1974, 559.
7. NOMINÉ, A. M., BÉDÈRE, D. and MIANNAY, D., Third Int. Conf. on Fracture, Volume V, München, 1973.
8. POWELL, G. L., Journal of Physical Chemistry, to be published, 1976.
9. PETERSON, C. A. W., U.C.R.L. 14132, April, 1965.
10. WITLOW, G. A., AWRE Report No. 049/66, July, 1966.
11. NOMINÉ, A. M., LE POAC, P. and MIANNAY, D., Mem. Sc. Rev. Metall., to be published, 1976.
12. AUSTEN, I. M., BROOK, R. and WEST, J. M., Int. J. Fracture, 12, 1976, 253.
13. RICE, J. R. and TRACEY, D. M., Numerical and Computer Methods in Structural Mechanics, Academic Press, 1973, 585.
14. LINDLEY, T. C. and RICHARDS, C. E., Third Int. Conf. on Fracture, Volume VI, München, 1973.
15. HUDAK, S. J. and WEI, R. P., Met. Trans. A., 7A, 1976, 235.
16. MAGNANI, N. J., Corrosion, NACE, 31, 1975, 337.

Table 1 Chemical Composition

Mo	C	N	O	H	Fe	Al	Si
wt %	ppm						
10.4	87	70	200	5	100	30	20

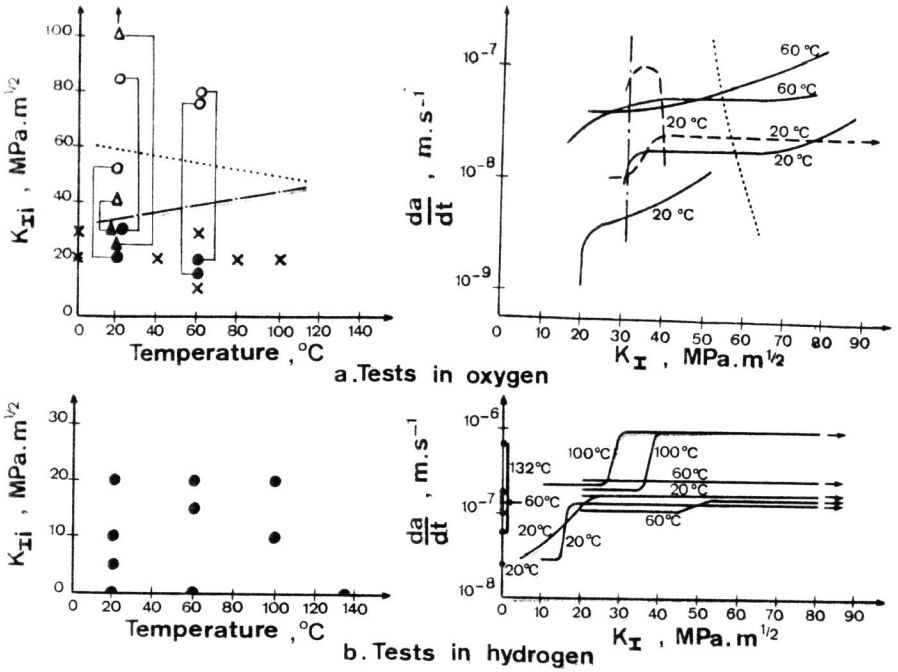

Figure 1 S.C.C. Map and Enhanced Crack Growth Rate (●, ▲, x: K_{Ii}; ○, △: K_{Is}; ●, ○, ————: Failed Under 0.15 MPa; ▲, △, --------: Failed Under 1,5 kPa; x: Unfailed Under 0,15 Mpa; .....: $K_I = \sqrt{B}\sigma_y$; —— - ——: K_{Ic})

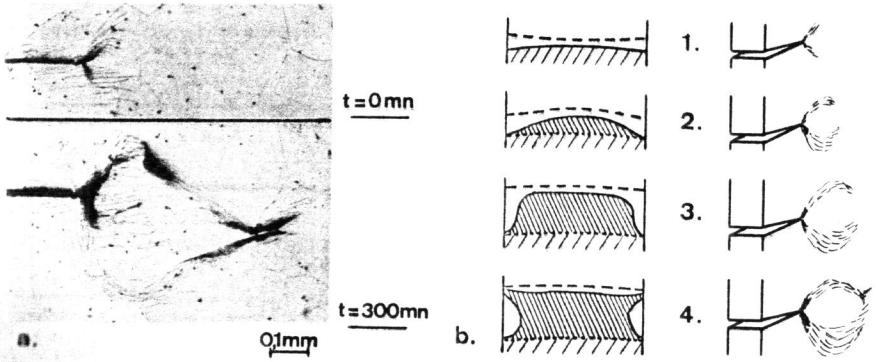

Figure 2 Example of Onset of Cracking in Oxygen and Schematic Diagram as seen from Above the Crack Plane and on the Observed Surface (//////: Fatigue Crack; \\\\\\ : S.C.C.; ————: Crack Tip; ---: Limit of Plastic Zone) (20 MPa•m$^{1/2}$, 60°C)

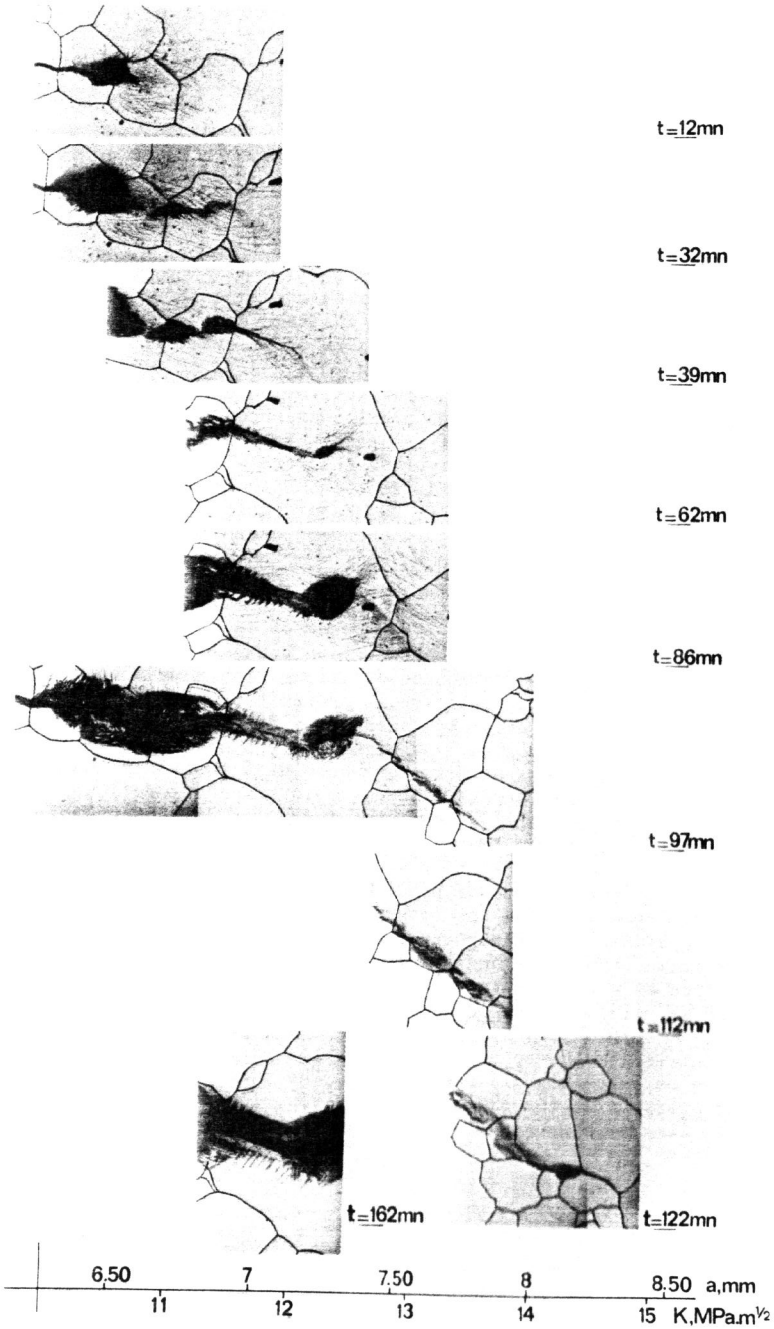

Figure 3 Sample of Crack Propagation in Hydrogen (10 MPa•m$^{1/2}$, 100°C)